

MULTIMODAL CONTROLLER FOR GENERATIVE MODELS

Enmao Diao¹, Jie Ding², Vahid Tarokh¹

¹ Department of Electrical and Computer Engineering, Duke University, Durham, NC, USA

² School of Statistics, University of Minnesota Twin Cities, Minneapolis, MN, USA

ABSTRACT

Class-conditional generative models are crucial tools for data generation from user-specified class labels. Existing approaches for class-conditional generative models require nontrivial modifications of backbone generative architectures to model conditional information fed into the model. This paper introduces a plug-and-play module named ‘multimodal controller’ to generate multimodal data without introducing additional learning parameters. In the absence of the controllers, our model reduces to non-conditional generative models. We test the efficacy of multimodal controller on CIFAR10, CIFAR100, COIL100, and Omniglot benchmark datasets. We demonstrate that multimodal controlled generative models (including VAE, PixelCNN, Glow, and GAN) can generate class-conditional images of significantly better quality when compared with the state-of-the-art conditional generative models. Moreover, we show that multimodal controlled models can also transit images between classes and create novel modalities of images.

Index Terms— Generative Models, Multimodal Learning, Computer Vision

1. INTRODUCTION

In recent years, many generative models based on neural networks have been proposed and achieved remarkable performance. The main backbones of generative models include Autoencoder, Autoregression, Normalization Flow, and Adversarial generative models. Perhaps the most well-known representatives of them are Variational Autoencoder (VAE) [1], PixelCNN [2], Glow [3], and Generative Adversarial Network (GAN) [4], respectively. VAE learns a parametric distribution over an encoded latent space, samples from this distribution, and then constructs generations from decoded samples. PixelCNN uses autoregressive connections to factorize the joint image distribution as a product of conditionals over sub-pixels. Glow optimizes the exact log-likelihood of the data with a deterministic and invertible transformation. GAN was introduced as a generative framework where intractable

probabilistic distributions are approximated through adversarial training.

In many application scenarios, we are interested in constructing generations based on a conditional distribution. For instance, we may be interested in generating human face images conditional on some given characteristics of faces such as hair color, eye size, gender, etc. A systematic way to incorporate conditional information may enable us to control the data generating process with more flexibility. In this direction, conditional generative models including Conditional Variational Autoencoder (CVAE) [5], Conditional Generative Adversarial Network (CGAN) [6], and Conditional PixelCNN (CPixelCNN) [7] have been proposed which model conditional information by learning the associated embeddings. The learned features are usually concatenated or added with non-conditional features at various network layers. Conditional Glow (CGlow) learns a class-conditional prior distribution and an optional auxiliary classifier.

In this paper, we propose a plug-and-play module named Multimodal Controller (MC) to allocate uniformly sampled subnetwork for each mode of data. Instead of introducing additional learning parameters to model conditional information, multimodal controlled generative models generate each mode of data from its corresponding unique subnetwork. Our main contributions of this work are three-fold.

- We provide a novel method to transform non-conditional generative models into class-conditional generative models, by simply attaching a multimodal controller at each layer. Unlike classical conditional generative models, our method does not introduce additional learning parameters, and it can be easily incorporated into existing implementations.
- We demonstrate that the multimodal controlled generative models can allocate specialized subnetworks to a substantial number of data modality. Our method outperforms various well-known classical conditional generative models for not-in-the-wild datasets with small intra-class variation and a large number of classes (i.e., COIL100, Omniglot) as shown in Table 3.
- We show that multimodal controlled generative models can transit between data modalities and create new

This work was supported by the Office of Naval Research (ONR) under grant number N00014-18-1-2244, and the Army Research Office (ARO) under grant number W911NF-20-1-0222.

modalities. Instead of using a convex combination of embeddings like classical conditional generative models, the multimodal controller can create novel subnetworks with genetic crossover and uniform sampling of a codebook.

We experiment with CIFAR10, CIFAR100, COIL100, and Omniglot datasets [8, 9, 10]. We compare our method with the conditional generative models with different backbone generative models such as VAE, PixelCNN, Glow, and GAN. The rest of the paper is organized as follows. In Section 2, we review the related work. In Section 3, we introduce our proposed multimodal controller. In Section 4, we provide experimental results demonstrating the performance of our approach. Finally, we make our concluding remarks in Section 5.

2. RELATED WORK

We use four distinct backbone generative models including Variational Autoencoder (VAE) [1], PixelCNN [2], Glow [3] and Generative Adversarial Network (GAN) [4] to demonstrate general compatibility of our method. VAE is a directed generative model with probabilistic latent variables. PixelCNN is an autoregressive generative model that fully factorizes the joint probability density function of images into a product of conditional distributions over all sub-pixels. Glow is a flow-based generative model that enables exact and tractable log-likelihood and latent space inference by ensuring a bijective neural network mapping. GAN consists of a Generator (G) network and a Discriminator (D) network that trains to find a Nash equilibrium for generating realistic-looking images.

Classical *conditional generative models* treat class-conditional information h as input to the model. Typically, modeling such h requires additional learning parameters and the resulting objective is the conditional distribution $p_\theta(x | h)$. Conditional VAE (CVAE) [5] and Conditional GAN (CGAN) [6] concatenate trainable embeddings to both encoder (discriminator) and decoder (generator). Apart from trainable embeddings, this approach also requires additional learning parameters on the backbone generative models to incorporate the embeddings. Instead of concatenating, Conditional PixelCNN (CPixelCNN) [2] and Conditional Glow (CGlow) [3] adds trainable embeddings to the features. This method requires the size of embedding to match the channel size of features. There also exist many other ways of modeling h . ACGAN [11] introduces an auxiliary classifier with a class-conditional objective function to model h . The Conditional Normalization [12, 13] learns class-conditional affine parameters, which can be considered another way to incorporate embeddings. [14] proposed a projection discriminator to mode h by measuring the cosine similarity between features and a learned embedding. A hybrid approach that combines

the previous two methods was used in BigGAN [15]. Recently, StyleGAN [16] enables scale-specific synthesis by transforming style information with fully connected layers into affine parameters for conditional normalization. MSGAN [17] models h to generate a mode-seeking regularization term. STGAN [18] enables image attribute editing by modeling the difference between the source and target h .

We aim to introduce a novel and generic alternative method to generate data class-conditionally. We term all methods mentioned above as conditional generative models because they all attempt to utilize a certain parametric module to model class-conditional information h , which are treated as an additional input to the model. Intuitively, training separate models for each mode of data can guarantee class-conditional data generation. However, we do not want the model complexity to grow with the number of classes. Recently, a few works pay attention to subnetworks. The lottery ticket hypothesis [19] states that there may exist a subnetwork that can match the performance of the original network when trained in isolation. PathNet [20] demonstrates successful transfer learning through migration from one subnetwork to the other. We propose *multimodal controlled generative models* to uniformly sample subnetworks from a backbone generative model and allocate a unique computational path for each data modality. The resulting objective is therefore $p_{\theta_h}(x)$. This paper empirically justifies the following claim. Uniformly sampled subnetworks can well-represent a substantial number of modalities by allocating a unique computational path for each mode of data.

3. MULTIMODAL CONTROLLER

Suppose that there is a dataset X with C data modality. Each mode of data $X_c = \{x_c^i\}_{i=1}^{N_c}$ consists of N_c i.i.d. samples of a (continuous or discrete) random variable. Given a set of learning model parameters $\theta \in \mathbb{R}^D$ with size D , each mode of data is modeled with a random subset $\theta_c \subset \theta$. For notational convenience, we will interchangeably use the notions of subset and subvector. In this way, the allocated parameters for each mode will represent both the inter-mode association and intra-mode variation thanks to parameter sharing and specialization.

Next, we discuss technical details in the specific context of neural networks. Suppose a uniformly sampled subnetwork takes input $X_c \in \mathbb{R}^{N_c \times K_c}$, where N_c and K_c are the batch size and the input channel size for data mode c . Suppose that the subnetwork is parameterized by a weight matrix $W_c \in \mathbb{R}^{D_c \times K_c}$ and bias vector $b_c \in \mathbb{R}^{D_c}$, where D_c is the output channel size for data mode c , then we have output $y_c \in \mathbb{R}^{N_c \times D_c}$ where

$$y_c = \phi(\text{BN}_c(X_c \times W_c^T + b_c))$$

$\text{BN}_c(\cdot)$ denotes the Batch Normalization (BN) [21] with affine parameters for corresponding data mode c and $\phi(\cdot)$ is

the activation function.

The computation cost of the above formulation increases with the number of data modalities, as we need to sequentially backward each subnetwork. Therefore we propose a nonparametric module named *multimodal controller* using a masking method similar to Dropout [22], which approximates model averaging with randomly sampled subnetworks.

We uniformly draw C unique modality codewords $e_c \in \mathbb{F}_2^D$ to construct a modality codebook $e \in \mathbb{F}_2^{C \times D}$, where \mathbb{F}_2 denotes the binary field. Note that each row of the codebook is a binary mask allocated for each mode of data. Let \times denote the usual matrix multiplication, and \odot denote the element-wise product. For notational brevity, given a matrix U and a vector u , we let $U \odot v$ denote $U \odot V$ where V is broadcast from u (if the dimension matches). A similar notion applies to the operations of multiplication and addition. Let $X \in \mathbb{R}^{N \times K}$ denote the output from the previous layer. Suppose that the original network is parameterized by a weight matrix $W \in \mathbb{R}^{D \times K}$ and bias vector $b \in \mathbb{R}^D$. Then for a specific mode of data c , we have output $y \in \mathbb{R}^{N \times D}$ where

$$\begin{aligned}\hat{W}_c &= W \odot e_c, \quad \hat{b}_c^D = b \odot e_c, \\ \hat{B}N_c &= BN \odot e_c, \quad \hat{\phi}_c(\cdot) = \phi(\cdot) \odot e_c \\ y &= \hat{\phi}_c(\hat{B}N_c(X \times \hat{W}_c^T + \hat{b}_c)) \\ &= \phi(BN(X \times W^T + b)) \cdot e_c\end{aligned}$$

Note that \hat{W}_c , \hat{b}_c^D , $\hat{B}N_c$ and $\hat{\phi}_c$ are uniformly masked from original network. We can factorize e_c to avoid interfering with the calculation of running statistics and activation function because $e_c^n = e_c$. Suppose we have class-conditional information $h \in \mathbb{F}_2^{N \times C}$ where each row is a one-hot vector. The above formation can be extended for all data modality to compute in parallel as follows

$$y = \phi(BN(X \times W^T + b)) \cdot (h \times e).$$

Suppose that the above formulation is for an intermediate layer. Then X is the output masked from the multimodal controller in the previous layer. Denote $\tilde{e}_c \in \mathbb{F}_2^K$ as the codeword for data mode c in previous multimodal controller, then the effective subnetwork weight matrix \tilde{W} is $W \odot (e_c \times \tilde{e}_c)$. Since each codeword is uniformly sampled, the size of \tilde{W} is approximately $\frac{1}{4}$ the original W . Indeed, the multimodal controller is a nonparametric computation module modulating model architecture and trading memory space for speedup in runtime. Although the above formulation only describes the interaction of multimodal controller and linear network. It can be readily extended to other parametric modules, such as convolution layers. We demonstrate the suggested way of attaching this plug-and-play module in practice in Figure 1.

4. EXPERIMENTS

This section demonstrates applications of multimodal controlled generative models to data generation, transition, and

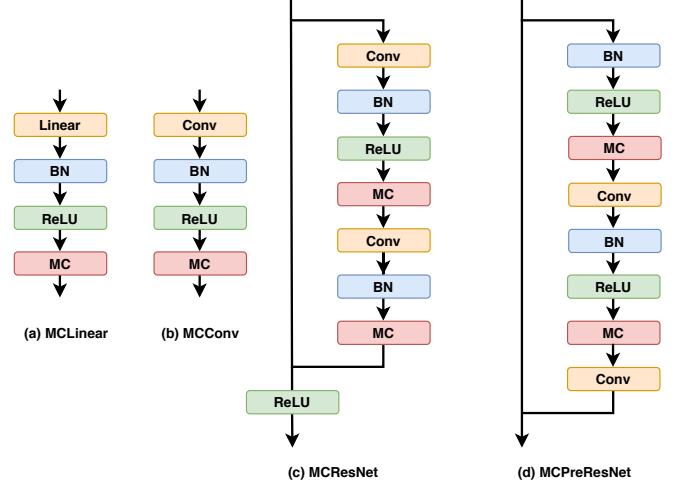


Fig. 1: Multimodal Controlled Neural Networks.

creation. We compare the result of our proposed method with that of classical conditional generative models. We illustrate our results for four different types of multimodal controlled generative models, including VAE, PixelCNN, Glow, and GAN on CIFAR10, CIFAR100, COIL100, and Omniglot datasets [8, 9, 10]. Due to our proposed method’s random nature, we conduct 12 random experiments for each generative model on each dataset. The standard errors in parentheses show that uniformly sampled subnetworks are robust enough to produce stable results for either a small or large number of data modality. Details regarding the experimental settings and network architecture for comparisons are described in the supplementary document.

Evaluating generative models is generally challenging [23]. Throughout our experiments, we use the Inception Score (IS) [24] and Fréchet Inception Distance (FID) [25] in order to approximately measure the quality of generated samples and to compare with the baseline. We also provide likelihood measurements for VAE, PixelCNN, and Glow in Table 1. The results show that multimodal controlled generative models perform comparably to conditional generative models in likelihood estimation.

	CIFAR10	CIFAR100	COIL100	Omniglot
CVAE	0.6 (0.00)	0.5 (0.00)	0.4 (0.00)	0.1 (0.00)
MCVAE	0.6 (0.00)	0.5 (0.00)	0.4 (0.00)	0.1 (0.00)
CPixelCNN	2.8 (0.11)	2.5 (0.14)	0.1 (0.00)	0.1 (0.05)
MCPixelCNN	3.0 (0.12)	2.7 (0.15)	0.1 (0.01)	0.5 (0.15)
CGlow	3.3 (0.00)	3.3 (0.01)	1.6 (0.03)	0.8 (0.01)
MCGlow	3.4 (0.01)	3.4 (0.01)	1.5 (0.02)	0.9 (0.01)

Table 1: Negative Log-Likelihood (NLL) of multimodal controlled and conditional VAE, PixelCNN and Glow.

	CIFAR10	CIFAR100	COIL100	Omniglot
CVAE	7.8	7.8	7.8	7.9
MCVAE	7.6	7.6	7.6	7.6
CPixelCNN	6.4	6.8	6.8	12.6
MCPixelCNN	6.4	6.4	6.4	6.4
CGlow	22.0	22.0	22.0	15.8
MCGlow	22.0	22.0	22.0	15.7
CGAN	5.5	5.5	8.7	8.8
MCGAN	5.3	5.3	8.4	8.4

Table 2: Number of learning parameters used in generative models in M (millions).

4.1. Generation

In this section, we present quantitative and qualitative results of generations from conditional and multimodal controlled generative models. More results are included in the supplementary document. Based on our results, multimodal controlled generative models can generate samples of comparable or better fidelity and diversity compared with conditional counterparts. We report our quantitative results in Table 3 with Inception Score (IS) [24] and Fréchet Inception Distance (FID) [25] which are perhaps the two most common metrics for comparing generative models.

Both conditional and multimodal controlled generative models share the same backbone generative models for a fair comparison. Therefore, it is unrealistic to expect multimodal controlled generative models to outperform their conditional counterparts in all cases. It is possible for conditional generative models to introduce more learning parameters for incorporating embeddings and thus produce better results. Most generative models in our experiments have similar model complexity, as shown in Table 2.

Our quantitative results show that multimodal controlled generative models perform comparably with conditional generative models for the CIFAR10 dataset, which has sufficient shots for a small number of data modality. When the amount of data per mode decreases as in the CIFAR100 dataset, our method performs worse than conditional generative models because each uniformly sampled subnetwork takes in less amount of data. On the other hand, our method performs considerably better than the conditional generative models for COIL100 and Omniglot datasets. The major difference among them is that CIFAR10 and CIFAR100 have higher intra-class variation (in-the-wild dataset) than COIL100 and Omniglot do. As shown in Table 4, COIL100, and Omniglot clustered more closely within each data modality as their Davies-Bouldin Index (DBI) [26] are smaller than those of CIFAR10 and CIFAR100. Note that uniformly sampled subnetworks are using approximately a quarter of the number of learning parameters as the original network. Therefore,

it is difficult for a small subnetwork to learn a mode of data with large variation. When intra-class variation is small, each subnetwork can specialize in corresponding data modality due to its unique computational path, and thus produce better results. It is worth mentioning that CPixelCNN for Omniglot outperforms MCPixelCNN because it has almost twice the learning parameters as the latter (since the size of conditional embeddings increases with the number of data modality in CPixelCNN).

Our qualitative results regarding MCGAN for COIL100 and Omniglot datasets are shown in Figure 3(a) and Figure 4(a). The rotation of different objects of MCGAN for COIL100 is readily recognized. The intra-class variation and inter-class distinction of Of MCGAN for Omniglot can also be easily identified. CGAN performs worse than our method due to the class-conditional mode collapse, and the qualitative results can be found in the supplementary document. Note that the number of data modality of COIL100 and Omniglot dataset is 100 and 1623 while their data per mode is 72 and 20, respectively. The result shows that MCGAN is mode-collapse free due to its unique computational paths, and thus it is capable of generating high fidelity and diversity images for a few-shot dataset when the intra-class variation is small.

We show the learning curves of CGAN and MCGAN for COIL100 and Omniglot in Figure 2. The learning curves also show that MCGAN consistently outperforms CGAN for the dataset with small intra-class variations. Both our quantitative and qualitative results demonstrate the efficacy of our proposed multimodal controller.

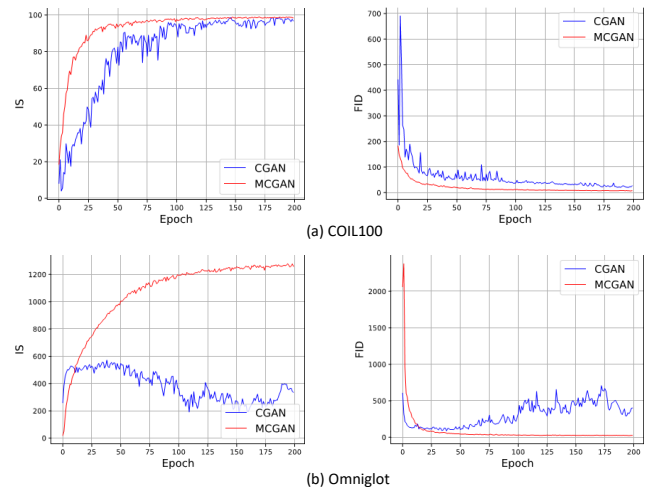


Fig. 2: Learning curves of CGAN and MCGAN for COIL100 and Omniglot datasets.

4.2. Transition

In this section, we provide qualitative results of data transition from multimodal controlled generative models. More re-

	CIFAR10		CIFAR100		COIL100		Omniglot	
	IS	FID	IS	FID	IS	FID	IS	FID
CVAE	3.4 (0.07)	133.7 (3.13)	3.5 (0.08)	130.9 (2.64)	89.4 (1.94)	37.6 (2.30)	539.8 (21.61)	367.5 (14.16)
MCVAE	3.4 (0.05)	128.6 (1.32)	3.0 (0.04)	144.3 (1.02)	95.2 (0.50)	29.5 (1.91)	889.3 (16.94)	328.5 (9.82)
CPixelCNN	5.1 (0.06)	70.8 (1.78)	5.2 (0.07)	74.1 (2.18)	94.2 (0.68)	8.1 (0.51)	1048.5 (160.33)	23.4 (5.38)
MCPixelCNN	4.8 (0.04)	75.2 (1.60)	4.7 (0.06)	83.8 (1.76)	98.1 (0.75)	4.7 (0.69)	762.4 (86.07)	43.3 (6.20)
CGlow	4.4 (0.05)	63.9 (1.34)	4.5 (0.06)	74.2 (1.19)	78.3 (2.25)	35.1 (2.67)	616.9 (6.71)	40.8 (1.28)
MCGLow	4.8 (0.05)	65.2 (1.21)	4.4 (0.06)	83.1 (1.15)	89.6 (1.63)	42.0 (5.19)	998.5 (29.10)	47.2 (2.69)
CGAN	8.0 (0.10)	18.1 (0.75)	8.5 (0.15)	22.6 (0.78)	97.9 (0.78)	24.4 (9.86)	677.3 (40.07)	51.0 (12.65)
MCGAN	7.9 (0.13)	21.4 (0.83)	7.2 (0.11)	35.5 (1.20)	98.8 (0.09)	7.8 (0.44)	1288.8 (5.38)	23.9 (0.73)

Table 3: Inception Score (IS) and Fréchet Inception Distance (FID) for generative models.

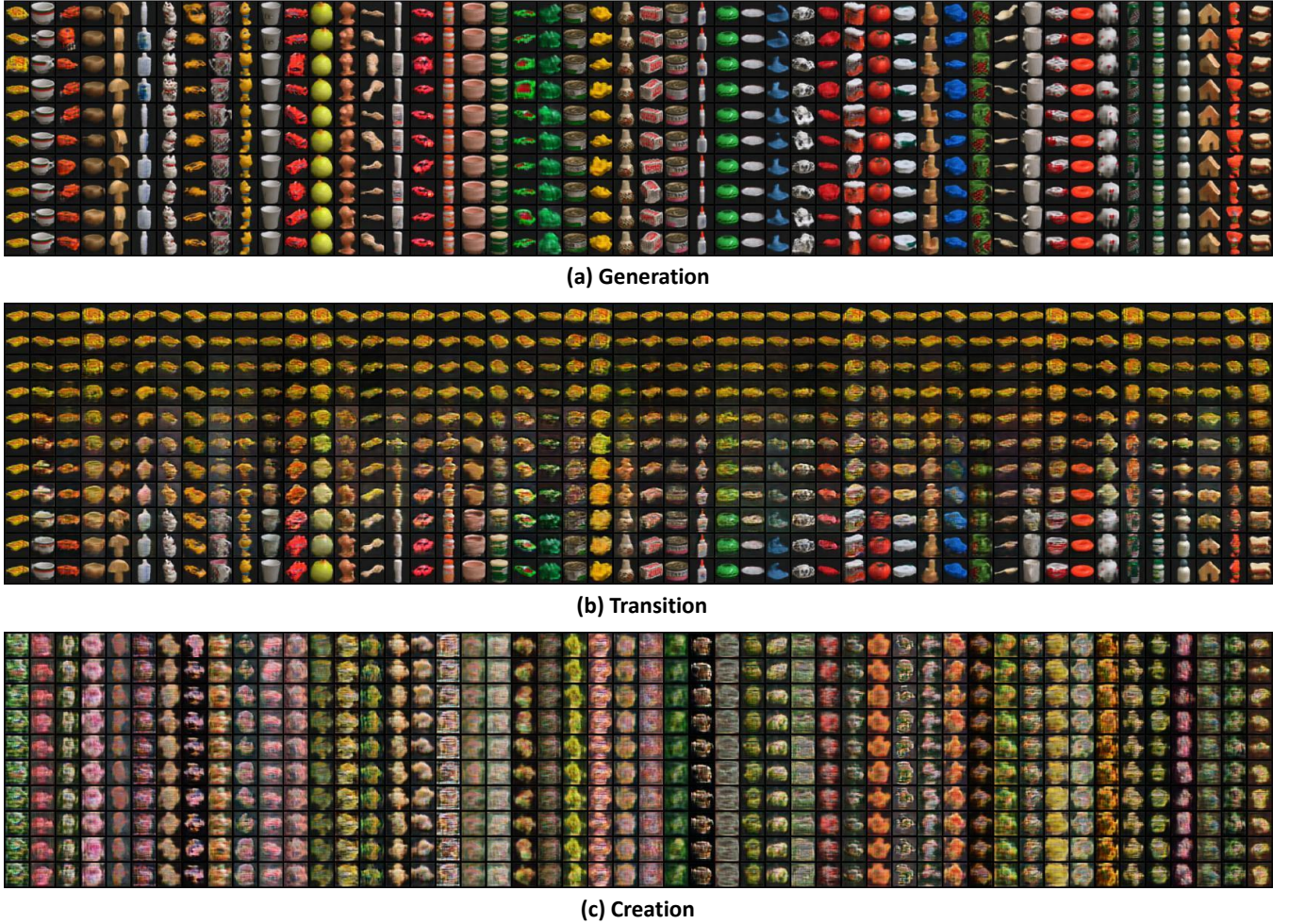
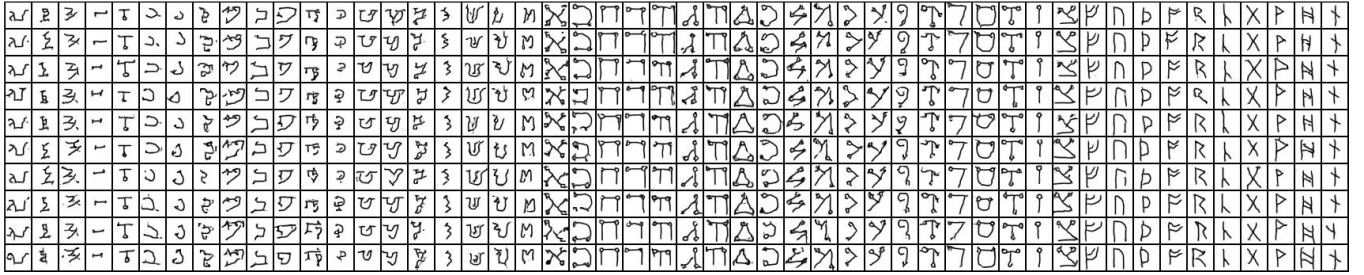


Fig. 3: (a) Generation (b) Transition (c) Creation from MCGAN trained with COIL100 dataset. (a) Generations in each column are from one data modality. (b) Transition in each column are from the first data modality to its corresponding data modality. (a) Creations in each column are from one uniformly sampled data modality. More results are included in the supplementary document.

	CIFAR10	CIFAR100	COIL100	Omniglot
Raw dataset	12.0	12.0	2.7	5.4
CVAE	37.9 (5.10)	24.8 (0.43)	15.5 (0.60)	8.5 (0.04)
MCVAE	2.1 (0.17)	5.0 (0.24)	1.8 (0.06)	3.0 (0.03)
CPixelCNN	27.6 (1.84)	21.6 (0.34)	17.9 (0.59)	9.0 (0.19)
MCPixelCNN	3.8 (0.34)	5.1 (0.19)	4.8 (0.18)	4.6 (0.19)
CGLOW	40.3 (5.09)	21.6 (0.26)	14.3 (0.87)	8.0 (0.02)
MCGlow	5.4 (0.46)	8.1 (0.21)	2.8 (0.12)	5.1 (0.14)
CGAN	33.2 (3.46)	20.5 (0.49)	10.4 (2.88)	7.8 (0.08)
MCGAN	2.0 (0.30)	4.9 (0.18)	1.5 (0.07)	3.6 (0.02)

Table 4: Davies-Bouldin Index (DBI) for conditional and multimodal controlled generative models on the raw and created datasets. The created dataset has the same number of modalities as the raw dataset. Small DBI values indicate that data creations are closely clustered on novel data modality. We note that the quantity of DBI does not fully characterize the ‘goodness’ of creation, and other possible evaluation criteria are left as future work.



(a) Generation



(b) Transition



(c) Creation

Fig. 4: (a) Generation (b) Transition (c) Creation from MCGAN trained with Omniglot dataset. (a) Generations in each column are from one data modality. (b) Transition in each column are from the first data modality to its corresponding data modality. (a) Creations in each column are from one uniformly sampled data modality. More results are included in the supplementary document.

sults are included in the supplementary document. For a given fixed latent vector z , VAE, Glow and GAN are able to transit one generated example from one data modality to another. Conditional generative models achieve this task by interpolating a convex combination between two selected embeddings. However, our model does not contain learned parameters to interpolate. Because each unique subnetwork generates from one data modality, multimodal generative models transit between two data modality by interpolating model architecture between two subnetworks. Their model architecture can be solely represented by their corresponding codewords. For a given interpolation step rate $\alpha \in [0, 1]$, multimodal controlled generative models transit data with genetic crossover between two selected codewords e_1 and e_2 as illustrated in Figure 5. In particular, the transited codeword e_i is given by

$$e_i = [e_{1,0:\lfloor \alpha D \rfloor}, e_{2,\lfloor \alpha D \rfloor:D}]$$

Our qualitative results regarding MCGAN for COIL100 and

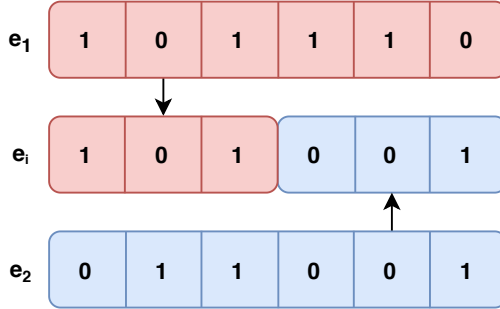


Fig. 5: Illustration of genetic crossover between codewords e_1 and e_2 to create intermediate transited codeword e_i .

Omniglot datasets are shown in Figure 3(b) and Figure 4(b). Note that our special way of transiting between data modality also demonstrates that our method is fundamentally different from conditional generative models. Intermediate subnetworks also have unique computation paths and thus we can also generate data from transited data modality.

4.3. Creation

In this section, we provide quantitative and qualitative results of data creation from conditional and multimodal controlled generative models. in Table 4. A generative model can class-conditionally synthesize from a novel data modality not even prescribed in the training dataset. We emphasize the distinction between data transition and creation here: a novel data modality is uniformly created from all the possible modalities instead of interpolating between two selected data modalities.

As mentioned in the previous section, conditional generative models can create data with a convex combination of embeddings. We can uniformly create new data modality by sampling convex combination from $\text{Dir}(1)$ distribution.

Because trained subnetworks are uniformly sampled, a natural way of uniformly creating new data modality for multimodal controlled generative models is to uniformly resample the codebook e .

We quantitatively evaluate the quality of data creation with Davies-Bouldin Index (DBI) [26], as shown in Table 4. Small DBI values indicate that data creations are closely clustered on novel data modality. Because novel data modalities are created from resampled subnetworks, multimodal controlled generative models can uniformly create closely clustered data. Conditional generative models have much higher DBI and thus fail to create clustered data.

Our qualitative results regarding MCGAN for COIL100 and Omniglot datasets are shown in Figure 3(c) and Figure 4(c). The results show that uniformly resampled subnetworks can create novel data from a data modality that has never been trained before. As shown in our supplementary document, though creations from a multimodal controlled generative model trained with CIFAR10 dataset cluster closely, they are not structurally similar to the original training data. A possible reason is that a small number of data modality is insufficient to learn adequate subnetworks variations. On the contrary, multimodal controlled generative models trained with CIFAR100, COIL100, and Omniglot can create novel data with high fidelity and diversity because the variations of subnetworks have been sufficiently exploited.

5. CONCLUSION

In this work, we proposed a plug-and-play nonparametric module named Multimodal Controller (MC) to equip generative models with class-conditional data generation. Unlike classical conditional generative models that introduce additional learning parameters to model class-conditional information, our method allocates a unique computation path for each data mode with a uniformly sampled subnetwork. The multimodal controller is a general method applicable to various well-known backbone generative models, and it works particularly well for a substantial number of modalities (e.g., the Omniglot challenge). We believe that this work will shed light on the use of subnetworks for large-scale and multimodal deep learning. An interesting future direction is to study how the subnetwork can be adapted for cooperative learning scenarios such as assisted learning [27], federated learning [28, 29], meta learning [30, 31], and transfer learning [32, 33].

6. REFERENCES

- [1] Diederik P Kingma and Max Welling, “Auto-encoding variational bayes,” *arXiv preprint arXiv:1312.6114*, 2013.
- [2] Aaron van den Oord, Nal Kalchbrenner, and Koray Kavukcuoglu, “Pixel recurrent neural networks,” *arXiv preprint arXiv:1601.06759*, 2016.
- [3] Durk P Kingma and Prafulla Dhariwal, “Glow: Generative flow with invertible 1x1 convolutions,” in *Advances in Neural Information Processing Systems*, 2018, pp. 10215–10224.
- [4] Ian Goodfellow, Jean Pouget-Abadie, Mehdi Mirza, Bing Xu, David Warde-Farley, Sherjil Ozair, Aaron Courville, and Yoshua Bengio, “Generative adversarial nets,” in *Advances in neural information processing systems*, 2014, pp. 2672–2680.
- [5] Kihyuk Sohn, Honglak Lee, and Xinchen Yan, “Learning structured output representation using deep conditional generative models,” in *Advances in neural information processing systems*, 2015, pp. 3483–3491.
- [6] Mehdi Mirza and Simon Osindero, “Conditional generative adversarial nets,” *arXiv preprint arXiv:1411.1784*, 2014.
- [7] Aaron Van den Oord, Nal Kalchbrenner, Lasse Espeholt, Oriol Vinyals, Alex Graves, et al., “Conditional image generation with pixelcnn decoders,” in *Advances in neural information processing systems*, 2016, pp. 4790–4798.
- [8] Alex Krizhevsky et al., “Learning multiple layers of features from tiny images,” 2009.
- [9] Sameer A Nene, Shree K Nayar, Hiroshi Murase, et al., “Columbia object image library (coil-100),” .
- [10] Brenden M Lake, Ruslan Salakhutdinov, and Joshua B Tenenbaum, “Human-level concept learning through probabilistic program induction,” *Science*, vol. 350, no. 6266, pp. 1332–1338, 2015.
- [11] Augustus Odena, Christopher Olah, and Jonathon Shlens, “Conditional image synthesis with auxiliary classifier gans,” in *Proceedings of the 34th International Conference on Machine Learning-Volume 70*. JMLR.org, 2017, pp. 2642–2651.
- [12] Vincent Dumoulin, Jonathon Shlens, and Manjunath Kudlur, “A learned representation for artistic style,” *arXiv preprint arXiv:1610.07629*, 2016.
- [13] Harm De Vries, Florian Strub, Jérémie Mary, Hugo Larochelle, Olivier Pietquin, and Aaron C Courville, “Modulating early visual processing by language,” in *Advances in Neural Information Processing Systems*, 2017, pp. 6594–6604.
- [14] Takeru Miyato and Masanori Koyama, “cgans with projection discriminator,” *arXiv preprint arXiv:1802.05637*, 2018.
- [15] Andrew Brock, Jeff Donahue, and Karen Simonyan, “Large scale gan training for high fidelity natural image synthesis,” *arXiv preprint arXiv:1809.11096*, 2018.
- [16] Tero Karras, Samuli Laine, and Timo Aila, “A style-based generator architecture for generative adversarial networks,” in *Proceedings of the IEEE Conference on Computer Vision and Pattern Recognition*, 2019, pp. 4401–4410.
- [17] Qi Mao, Hsin-Ying Lee, Hung-Yu Tseng, Siwei Ma, and Ming-Hsuan Yang, “Mode seeking generative adversarial networks for diverse image synthesis,” in *Proceedings of the IEEE Conference on Computer Vision and Pattern Recognition*, 2019, pp. 1429–1437.
- [18] Ming Liu, Yukang Ding, Min Xia, Xiao Liu, Errui Ding, Wangmeng Zuo, and Shilei Wen, “Stgan: A unified selective transfer network for arbitrary image attribute editing,” in *Proceedings of the IEEE Conference on Computer Vision and Pattern Recognition*, 2019, pp. 3673–3682.
- [19] Jonathan Frankle and Michael Carbin, “The lottery ticket hypothesis: Finding sparse, trainable neural networks,” *arXiv preprint arXiv:1803.03635*, 2018.
- [20] Chrisantha Fernando, Dylan Banarse, Charles Blundell, Yori Zwols, David Ha, Andrei A Rusu, Alexander Pritzel, and Daan Wierstra, “Pathnet: Evolution channels gradient descent in super neural networks,” *arXiv preprint arXiv:1701.08734*, 2017.
- [21] Sergey Ioffe and Christian Szegedy, “Batch normalization: Accelerating deep network training by reducing internal covariate shift,” *arXiv preprint arXiv:1502.03167*, 2015.
- [22] Nitish Srivastava, Geoffrey Hinton, Alex Krizhevsky, Ilya Sutskever, and Ruslan Salakhutdinov, “Dropout: a simple way to prevent neural networks from overfitting,” *The journal of machine learning research*, vol. 15, no. 1, pp. 1929–1958, 2014.
- [23] Lucas Theis, Aäron van den Oord, and Matthias Bethge, “A note on the evaluation of generative models,” *arXiv preprint arXiv:1511.01844*, 2015.

- [24] Tim Salimans, Ian Goodfellow, Wojciech Zaremba, Vicki Cheung, Alec Radford, and Xi Chen, “Improved techniques for training gans,” in *Advances in neural information processing systems*, 2016, pp. 2234–2242.
- [25] Martin Heusel, Hubert Ramsauer, Thomas Unterthiner, Bernhard Nessler, and Sepp Hochreiter, “Gans trained by a two time-scale update rule converge to a local nash equilibrium,” in *Advances in neural information processing systems*, 2017, pp. 6626–6637.
- [26] David L Davies and Donald W Bouldin, “A cluster separation measure,” *IEEE transactions on pattern analysis and machine intelligence*, , no. 2, pp. 224–227, 1979.
- [27] Xun Xian, Xinran Wang, Jie Ding, and Reza Ghanadan, “Assisted learning: a framework for multi-organization learning,” *NeurIPS 2020 (spotlight)*, 2020.
- [28] Jakub Konečný, H Brendan McMahan, Felix X Yu, Peter Richtárik, Ananda Theertha Suresh, and Dave Bacon, “Federated learning: Strategies for improving communication efficiency,” *arXiv preprint arXiv:1610.05492*, 2016.
- [29] Brendan McMahan, Eider Moore, Daniel Ramage, Seth Hampson, and Blaise Agüera y Arcas, “Communication-efficient learning of deep networks from decentralized data,” in *Artificial Intelligence and Statistics*. PMLR, 2017, pp. 1273–1282.
- [30] Yihan Jiang, Jakub Konečný, Keith Rush, and Sreeram Kannan, “Improving federated learning personalization via model agnostic meta learning,” *arXiv preprint arXiv:1909.12488*, 2019.
- [31] Mikhail Khodak, Maria-Florina F Balcan, and Ameet S Talwalkar, “Adaptive gradient-based meta-learning methods,” in *Advances in Neural Information Processing Systems*, 2019, pp. 5917–5928.
- [32] Kangkang Wang, Rajiv Mathews, Chloé Kiddon, Hubert Eichner, Françoise Beaufays, and Daniel Ramage, “Federated evaluation of on-device personalization,” *arXiv preprint arXiv:1910.10252*, 2019.
- [33] Yishay Mansour, Mehryar Mohri, Jae Ro, and Ananda Theertha Suresh, “Three approaches for personalization with applications to federated learning,” *arXiv preprint arXiv:2002.10619*, 2020.
- [34] Christian Szegedy, Wei Liu, Yangqing Jia, Pierre Sermanet, Scott Reed, Dragomir Anguelov, Dumitru Erhan, Vincent Vanhoucke, and Andrew Rabinovich, “Going deeper with convolutions,” in *Proceedings of the IEEE conference on computer vision and pattern recognition*, 2015, pp. 1–9.
- [35] Aaron van den Oord, Oriol Vinyals, et al., “Neural discrete representation learning,” in *Advances in Neural Information Processing Systems*, 2017, pp. 6306–6315.
- [36] Kaiming He, Xiangyu Zhang, Shaoqing Ren, and Jian Sun, “Identity mappings in deep residual networks,” in *European conference on computer vision*. Springer, 2016, pp. 630–645.
- [37] Laurent Dinh, Jascha Sohl-Dickstein, and Samy Bengio, “Density estimation using real nvp,” *arXiv preprint arXiv:1605.08803*, 2016.
- [38] Takeru Miyato, Toshiki Kataoka, Masanori Koyama, and Yuichi Yoshida, “Spectral normalization for generative adversarial networks,” *arXiv preprint arXiv:1802.05957*, 2018.

Appendix

In this supplementary document, we provide 1) more experimental details including the metrics and network architecture, 2) more qualitative results to demonstrate the multimodal controlled generative models presented in the main paper as well as conditional generative models. Our codes and comments to reproduce the presented results have been uploaded as part of the supplementary material.

6.1. Experimental Details

6.1.1. Metric

Inception Score (IS) was originally introduced by [24] and formulated as

$$\exp [\mathbb{E} \{D_{\text{KL}}(p(y|x)||p(y))\}]$$

where $p(y|x)$ is the output of pretrained Inception network [34]. It is known that IS is strongly correlated with subjective human views of image quality. Fréchet Inception Distance (FID) [25] uses the information of the final layer of the inception model to measure the quality of the generated examples. It measures the Wasserstein distance between two distributions p_1 and p_2 assuming that they are both multivariate Gaussian distributions, expressed by

$$\|\mu_{p_1} - \mu_{p_2}\|_2^2 + \text{trace} \left(C_{p_1} + C_{p_2} - 2(C_{p_1}C_{p_2})^{1/2} \right),$$

where (μ_{p_1}, μ_{p_2}) and (C_{p_1}, C_{p_2}) are the mean and covariance of samples from p_1 and p_2 respectively.

We evaluate IS for CIFAR10 and CIFAR100 datasets with the standard Inception network pre-trained with the ImageNet dataset. We train our classifier as shown in Table 11 for COIL100 and Omniglot datasets with all the training and test data. We calculate the scores from randomly generated 1000 examples per data mode for CIFAR10, 100 for CIFAR100, 100 for COIL100, and 20 for the Omniglot dataset respectively. We repeat each experiment 12 times with different random seeds and report the mean and standard deviations (in brackets) as in Table 3.

6.1.2. Network Architecture

We show hyperparameters for training generative models in Table 12. The network architectures of MCVAE and MCGAN used in our experiments are shown in Table 5 to 10, where n_c is the number of image channels and M is the shape of the input image. We use VQVAE to reduce the computational complexity of PixelCNN. We use the exponential moving average to update the vector quantizer in VQVAE with a dictionary size of 512 and embedding dimension of 64 [35]. We use the standard architecture of PixelCNN and Glow described in the original work [7, 3]. The number of layers, embedding size, and hidden channel size of PixelCNN are 15,

512, and 128 respectively. The depth of flows K , the number of levels L , and the hidden channel size of Glow are 3, 16, and 512 respectively. We do not train an auxiliary classifier for Glow networks for fair comparisons with other generative models.

We show that the number of learning parameters of generative models in Table 2. The embedding size of embeddings used for modeling conditional information h in CVAE and CGAN is 32. We concatenate conditional embeddings to the first layer of the encoder (discriminator) and decoder (generator) as described in [5, 6]. Following the implementation suggested in [7], we add conditional embeddings to every gated activation in CPixelCNN. As a result, CPixelCNN has more learning parameters for modeling h than other conditional generative models do. As a result, the CPixelCNN for Omniglot also has twice the number of learning parameters as MCPixelCNN does. It is foreseeable that the CPixelCNN for Omniglot outperforms the MCPixelCNN as shown in 3. We add conditional embeddings to the trained prior in the first level of CGlow [3]. Multimodal controlled generative models always have less learning parameters than conditional generative models because we do not train any additional learning parameters and the uniformly sampled codebook e is merely an indicator for modulating subnetworks.

Multimodal controlled generative models attach the multimodal controller to various parametric layers, with some customization depending on their architectures. By controlling the allocation of subnetworks, uniformly sampled subnetworks are able to synthesize class-conditional data. We describe the usage of the multimodal controller for the most well-known representatives of generative models including VAE, PixelCNN, Glow, and GAN.

Multimodal Controlled Variational Autoencoder (MCVAE). MCVAE appends a multimodal controller to every layer of VAE. The number of model parameters remains the same as non-conditional VAE. If $e = \mathbf{1}$, the all-one matrix, our proposed method produces a non-conditional VAE. For each mode of data x_c , we allocate a unique subnetwork with learning parameters θ_c uniformly sampled from the overall model parameters θ , and we also obtain class-conditional latent variables z_c . The objective can be written as:

$$\min_{\theta} \left\{ \sum_{c=1}^C \frac{N_c}{N} \left[\mathbb{E}_{q_{\theta_c}(z_c|x_c)} \log p_{\theta_c}(x_c|z_c) - D_{\text{KL}}(q_{\theta_c}(z_c|x_c)||p_{\theta_c}(z_c)) \right] \right\}.$$

Thanks to the end-to-end structure of VAE, MCVAE can uniformly sample subnetworks by appending a multimodal controller after every parametric layer. For the bottleneck layer, we obtain class-conditional latent variables z_c by attaching the multimodal controller after applying the reparameterization trick, instead of directly attaching to the parameters of the latent distribution. The subnetworks θ_c can be optimized

in the same way as in non-conditional VAE.

Multimodal Controlled PixelCNN (MCPixelCNN).

PixelCNN combines two gated convolutional network stacks in order to remove blind spots in the receptive field [7]. MCPixelCNN allocates subnetworks for each data mode by introducing the following multimodal controlled gated activation unit:

$$y = \{ \tanh(W_{k,f} * x) \odot (h \times e) \} \odot \sigma(W_{k,g} * x),$$

where σ denotes the sigmoid function, k is the number of layers, and $*$ is the convolution operator. Our various experimental results show that controlling the $\tanh(\cdot)$ activation unit is sufficient for synthesizing class-conditional data. Other convolution layers used in connecting two stacks and residuals do not necessarily need to be multimodally controlled. The class-conditional likelihood function can be written as

$$\begin{aligned} p_{\theta_c}(x_c) &= p_{\theta_c}(x_{1,c}, \dots, x_{n,c}) \\ &= \prod_{i=1}^n p_{\theta_c}(x_{i,c} | x_{1,c}, \dots, x_{i-1,c}) \end{aligned}$$

Multimodal Controlled Glow (MCGlow). Glow has three major components including Actnorm, Invertible 1×1 convolution, and affine coupling layer. The number of channels of features passing Actnorm and Invertible 1×1 convolution is usually a multiple of the number of color channels due to the squeeze operation. It leads to a small number of channels of features which are incapable of allocating subnetworks for a large number of data modalities. MCGlow allocates subnetworks only for $\text{NN}(\cdot)$ in affine coupling layer, where $\text{NN}(\cdot)$ is a shallow and wide convolutional neural network block often used in ResNet [36] and RealNVP [37]. As a result, the parameters used in Actnorm and Invertible 1×1 convolution are shared across all data modalities. The class-conditional likelihood function for a k -layer Glow can be written as:

$$\begin{aligned} \log p_{\theta_c}(x_c) &= \log p(z) + \sum_{i=1}^k \log |\det(J(f_{i,c}^{-1}(x_c)))| \\ z &= f_{k,c}^{-1} \circ f_{k-1,c}^{-1} \circ \dots \circ f_{0,c}^{-1}(x_c). \end{aligned}$$

Multimodal Controlled Generative Adversarial Network (MCGAN). MCGAN appends a multimodal controller after every layer of the discriminator and generator. We experimentally found that using the multimodal controller on either generator or discriminator only does not produce a class-conditional synthesis. The objective function of a multimodal controlled two-player minimax game is formulated as:

$$\min_G \max_D \left\{ \sum_{c=1}^C \frac{N_c}{N} \left[\mathbb{E}_{q_{\theta_c}(x_c)} [\log D_{\theta_c}(x_c)] + \mathbb{E}_{p_{\theta_c}(z)} [\log(1 - D_{\theta_c}(G_{\theta_c}(z)))] \right] \right\}.$$

Image $x \in \mathbb{R}^{n_c \times M \times M}$
MCCConv ($n_c, 64, 4, 2, 1$)
MCCConv ($64, 128, 4, 2, 1$)
MCCConv ($128, 256, 4, 2, 1$)
MResBlock ($256, 256, 3, 1, 1$)
MResBlock ($256, 256, 3, 1, 1$)
Linear (μ) ($256 \times 4 \times 4, 128$)
Linear ($\log \sigma^2$) ($256 \times 4 \times 4, 128$)

Table 5: Encoder used in MCVAE for all datasets.

$z \in \mathbb{R}^{128} \sim \mathcal{N}(0, I)$
MC ($128, 128$)
Linear ($128, 256 \times 4 \times 4$), BN, ReLU
MC ($256, 256$)
MResBlock ($256, 256, 3, 1, 1$)
MResBlock ($256, 256, 3, 1, 1$)
MCCConvTranspose ($256, 128, 4, 2, 1$)
MCCConvTranspose ($128, 64, 4, 2, 1$)
ConvTranspose ($64, n_c, 4, 2, 1$), Sigmoid

Table 6: Decoder used in MCVAE for all datasets.

$z \in \mathbb{R}^{128} \sim \mathcal{N}(0, I)$
MCLinear ($128, 256 \times 4 \times 4$)
MCPReResBlock Up ($256, 256, 3, 1, 1$)
MCPReResBlock Up ($256, 256, 3, 1, 1$)
MCPReResBlock Up ($256, 256, 3, 1, 1$)
BN, ReLU, Conv ($256, n_c, 3, 1, 1$), Tanh

Table 7: Generator used in MCGAN for CIFAR10 and CIFAR100 datasets. ResBlock Up interpolates input feature map at the beginning of block by scale 2.

Image $x \in \mathbb{R}^{M \times M \times n_c}$
MCPreResBlock Down (n_c , 128, 3, 1, 1)
MCPreResBlock Down (128, 128, 3, 1, 1)
MCPreResBlock (128, 128, 3, 1, 1)
MCPreResBlock (128, 128, 3, 1, 1)
ReLU, Global Sum Pooling
Linear (512, 1)

Table 8: Discriminator used MCGAN for CIFAR10 and CIFAR100 datasets. All BN layers are replaced with Spectral Normalization (SN) [38]. ResBlock Down average pools feature map at the end of block by scale 2.

$z \in \mathbb{R}^{128} \sim \mathcal{N}(0, I)$
MCLinear (128, $512 \times 4 \times 4$)
MCPreResBlock Up (512, 256, 3, 1, 1)
MCPreResBlock Up (256, 128, 3, 1, 1)
MCPreResBlock Up (128, 64, 3, 1, 1)
BN, ReLU, Conv (64, n_c , 3, 1, 1), Tanh

Table 9: Generator used in MCGAN for COIL100 and Omniglot datasets. ResBlock Up interpolates input feature map at the beginning of block by scale 2.

Image $x \in \mathbb{R}^{n_c \times M \times M}$
MCPreResBlock Down (n_c , 64, 3, 1, 1)
MCPreResBlock Down (64, 128, 3, 1, 1)
MCPreResBlock Down (128, 256, 3, 1, 1)
MCPreResBlock (256, 512, 3, 1, 1)
ReLU, Global Sum Pooling
Linear (512, 1)

Table 10: Discriminator used MCGAN for COIL100 and Omniglot datasets. All BN layers are replaced with Spectral Normalization (SN) [38]. ResBlock Down average pools feature map at the end of block by scale 2.

Image $x \in \mathbb{R}^{n_c \times M \times M}$
Conv (n_c , 8, 3, 1, 1)
MaxPool (8, 8, 2)
Conv (8, 16, 3, 1, 1)
MaxPool (16, 16, 2)
Conv (16, 32, 3, 1, 1)
MaxPool (32, 32, 2)
Conv (32, 64, 3, 1, 1)
Linear ($64 \times 4 \times 4$, C)

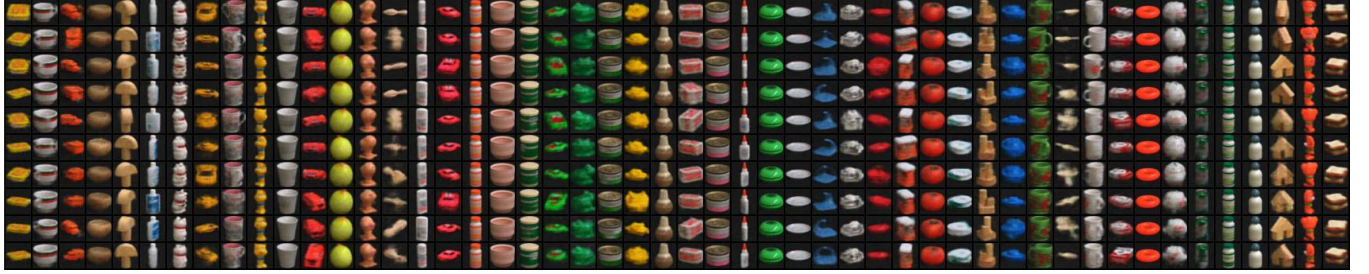
Table 11: Classifier used to train COIL100 and Omniglot for evaluating IS and FID.

Qualitative Results

In this section, we provide all qualitative results from our experiments in Figure 6 to 37. The qualitative results are well aligned with the quantitative results as shown in Table 3. For example, conditional generative models trained with the COIL100 dataset are not able to produce diverse orientation of objects. For CIFAR10 and CIFAR100 datasets, transitions from conditional generative models are stabler because each intermediate transition from multimodal generative models is generated from a unique subnetwork. Results from Glow suffer from numerical overflow (black areas) due to its invertibility. As mentioned in the main paper, if the number of data modality is as small as the CIFAR10 dataset, uniform data creations from multimodal generative models are not structurally similar to the original training data. Due to the unique subnetwork allocated for each mode of data, the qualitative results show that creations from multimodal generative models are more closely clustered than those from conditional generative models.

	Batch size	Loss	Optimizer	Learning rate	beta
VQVAE	128	MSE	Adam	3E-4	(0.9,0.999)
CVAE	128	BCE	Adam	3E-4	(0.9,0.999)
MCVAE	128	BCE	Adam	3E-4	(0.9,0.999)
CPixelCNN	128	NLL	Adam	3E-4	(0.9,0.999)
MCPixelCNN	128	NLL	Adam	3E-4	(0.9,0.999)
CGlow	128	NLL	Adam	3E-4	(0.9,0.999)
MCGlow	128	NLL	Adam	3E-4	(0.9,0.999)
CGAN	128	Hinge	Adam	2E-4	(0,0.9)
MCGAN	128	Hinge	Adam	2E-4	(0.5,0.999)

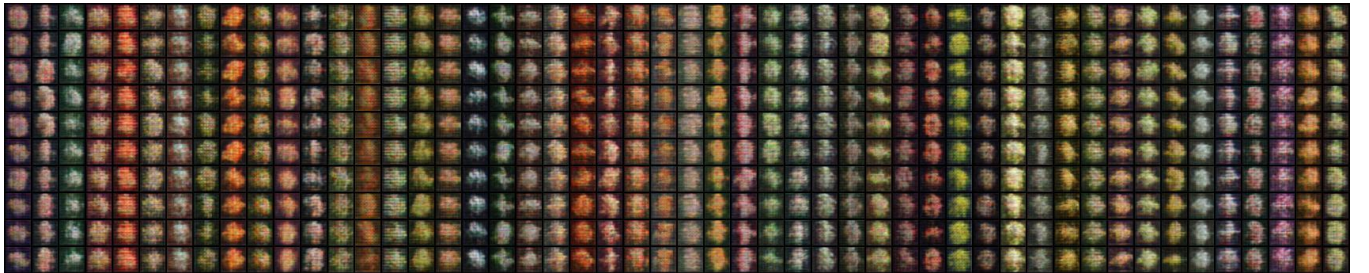
Table 12: Hyperparameters for training generative models.



(a) Generation

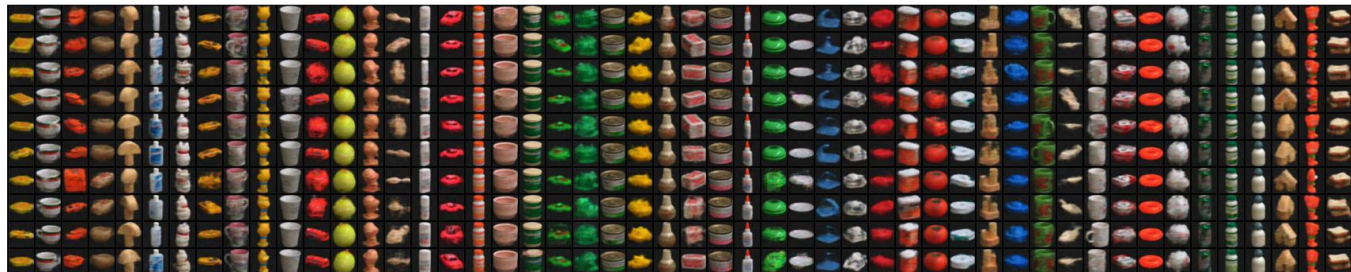


(b) Transition



(c) Creation

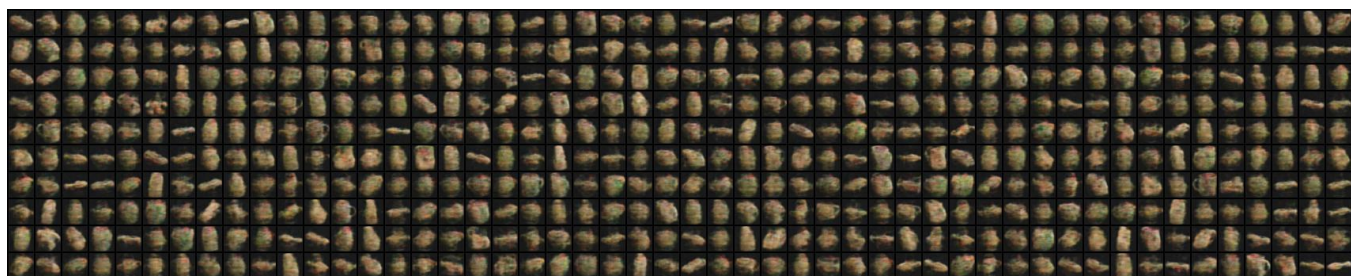
Fig. 6: (a) Generation (b) Transition (c) Creation from MCVAE trained with COIL100 dataset.



(a) Generation

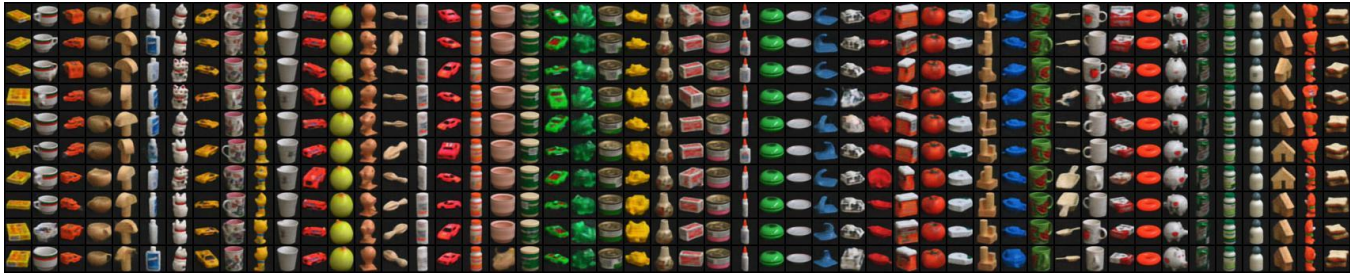


(b) Transition



(c) Creation

Fig. 7: (a) Generation (b) Transition (c) Creation from CVAE trained with COIL100 dataset.

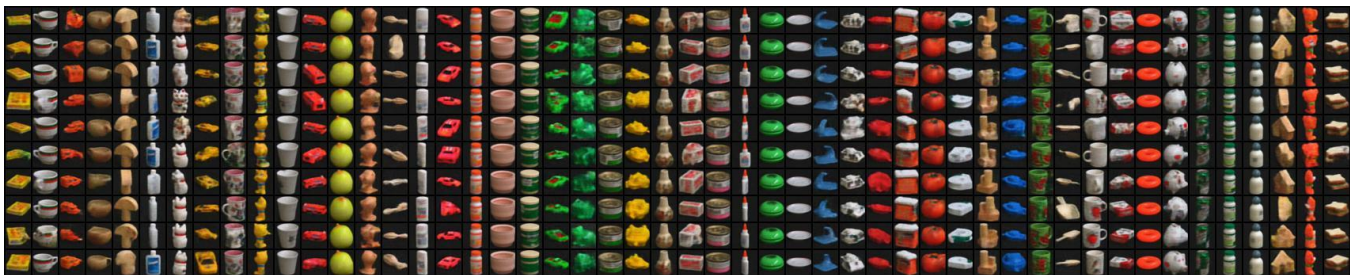


(a) Generation



(b) Creation

Fig. 8: (a) Generation (b) Transition (c) Creation from MCPixelCNN trained with COIL100 dataset.



(a) Generation



(b) Creation

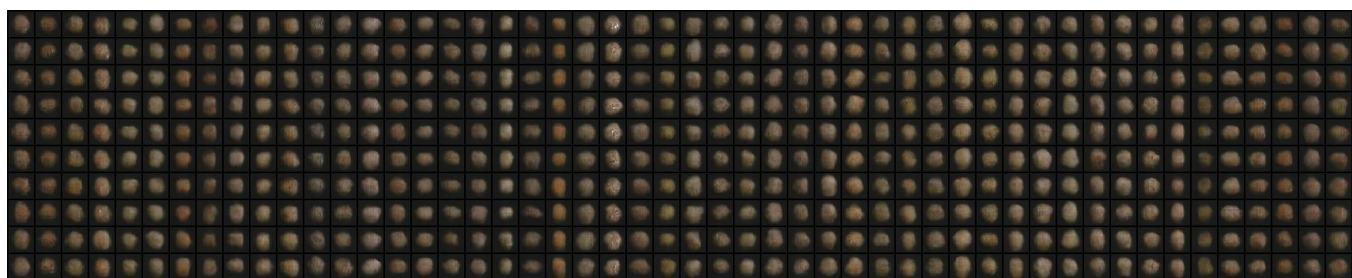
Fig. 9: (a) Generation (b) Transition (c) Creation from CPixelCNN trained with COIL100 dataset.



(a) Generation

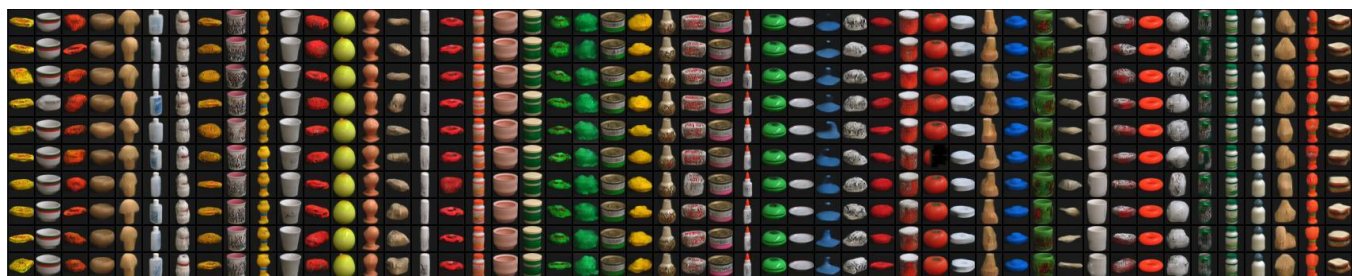


(b) Transition



(c) Creation

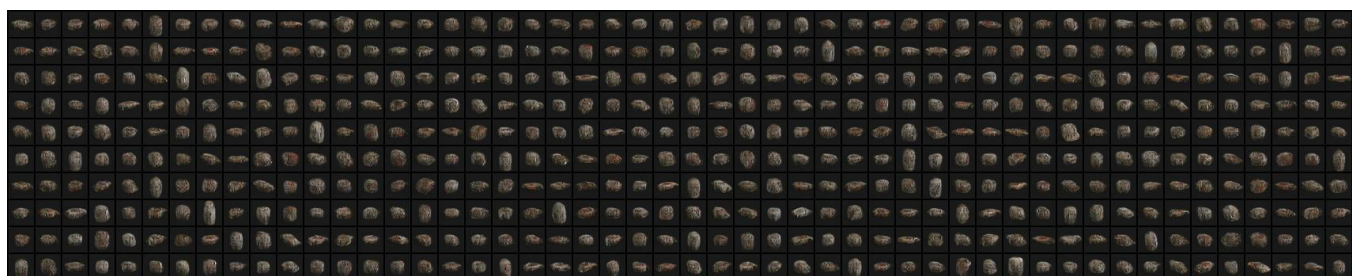
Fig. 10: (a) Generation (b) Transition (c) Creation from MCGlow trained with COIL100 dataset.



(a) Generation



(b) Transition

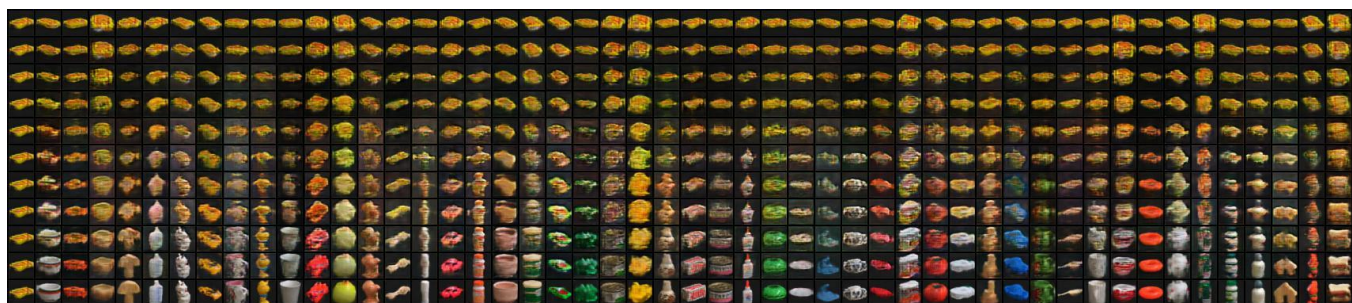


(c) Creation

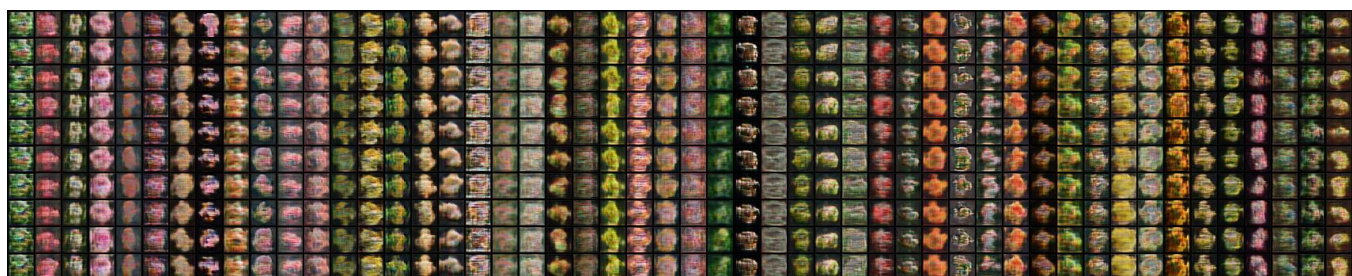
Fig. 11: (a) Generation (b) Transition (c) Creation from CGlow trained with COIL100 dataset.



(a) Generation



(b) Transition



(c) Creation

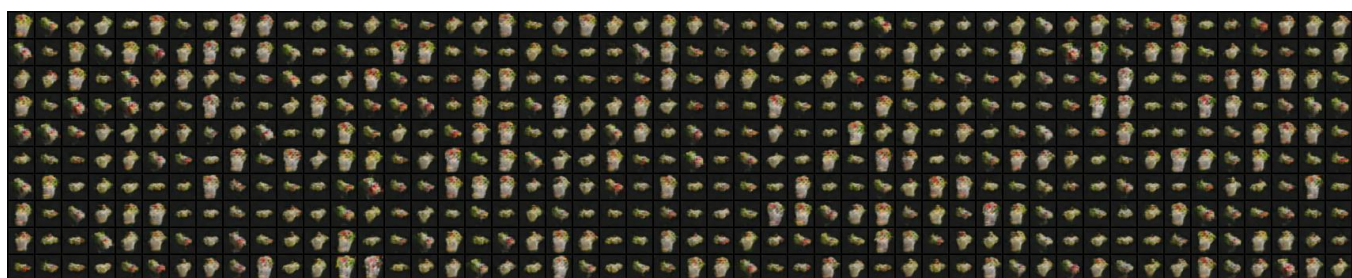
Fig. 12: (a) Generation (b) Transition (c) Creation from MCGAN trained with COIL100 dataset.



(a) Generation



(b) Transition



(c) Creation

Fig. 13: (a) Generation (b) Transition (c) Creation from CGAN trained with COIL100 dataset.

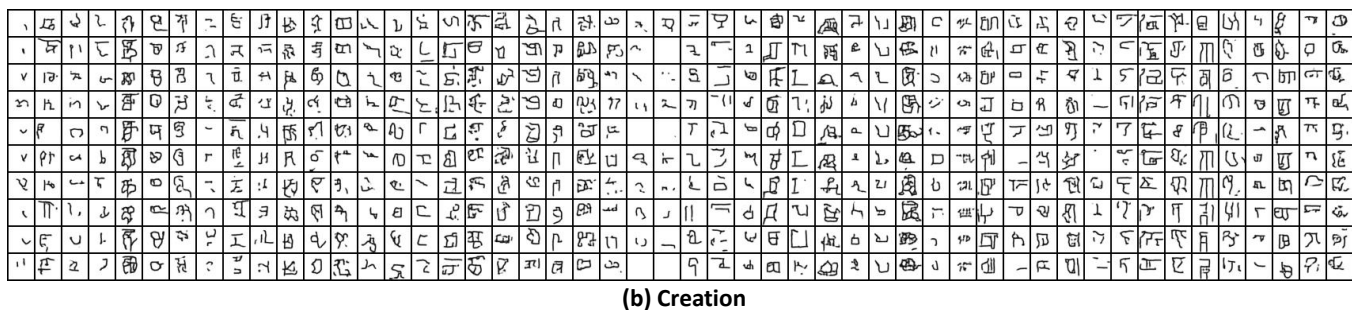
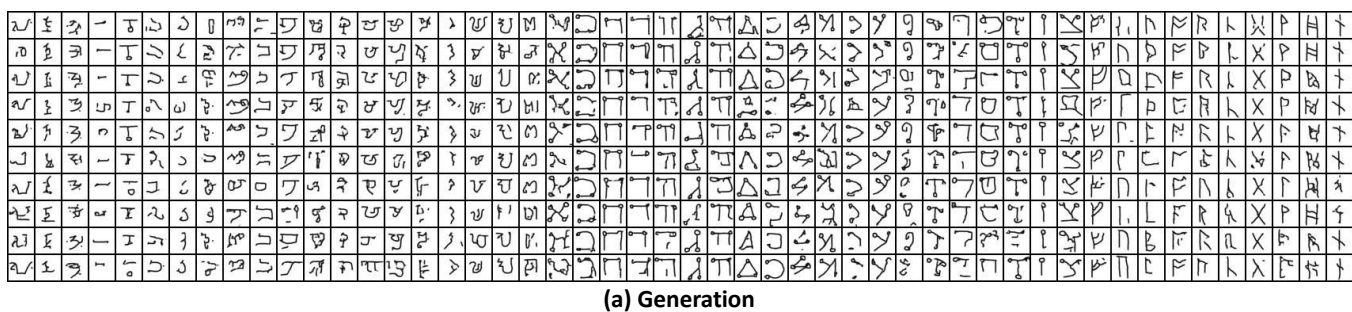


Fig. 16: (a) Generation (b) Transition (c) Creation from MCPixelCNN trained with Omniglot dataset.

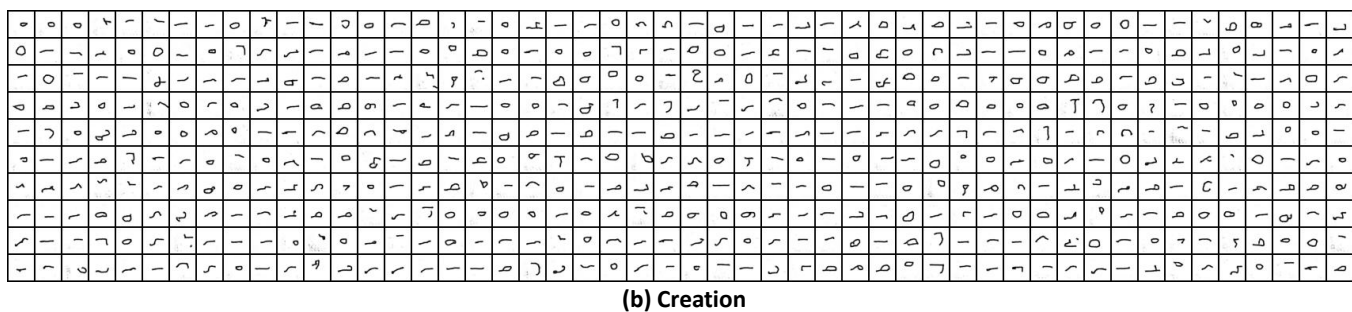
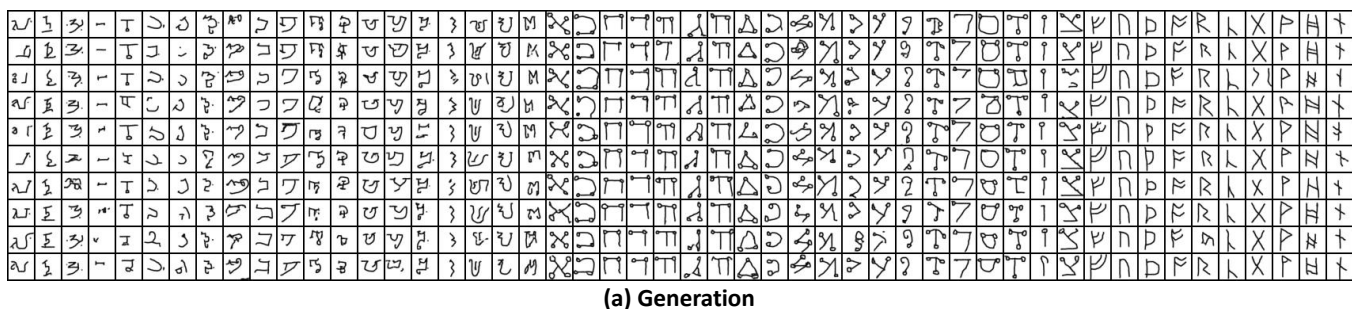
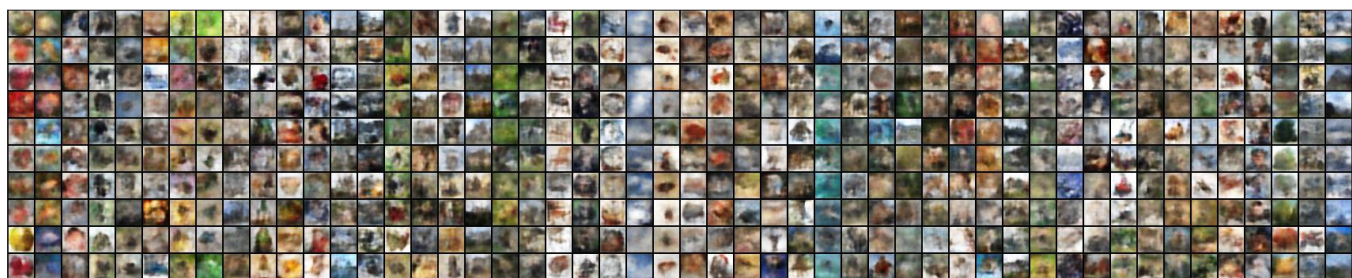
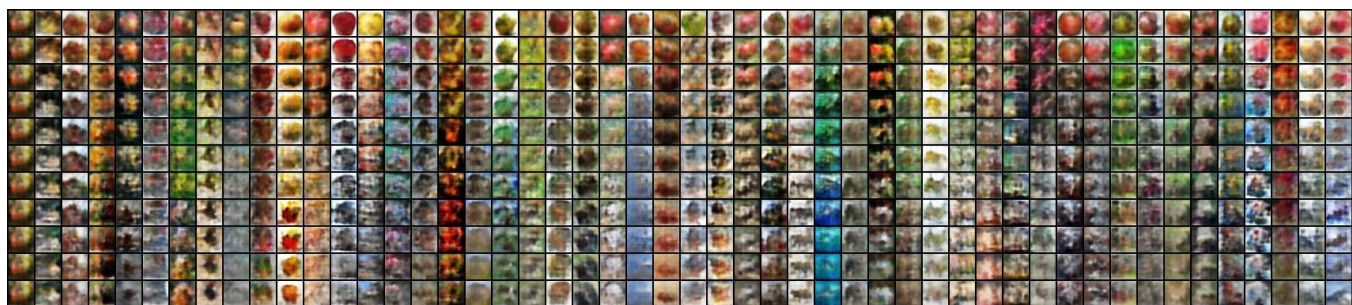


Fig. 17: (a) Generation (b) Transition (c) Creation from CPixelCNN trained with Omniglot dataset.



(a) Generation

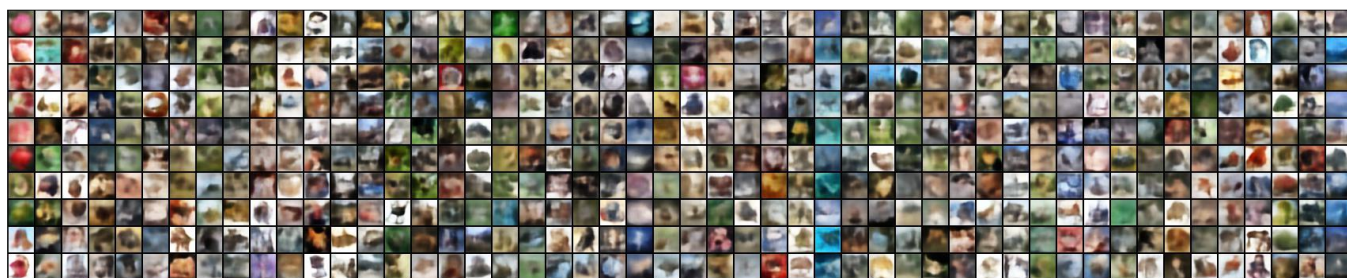


(b) Transition

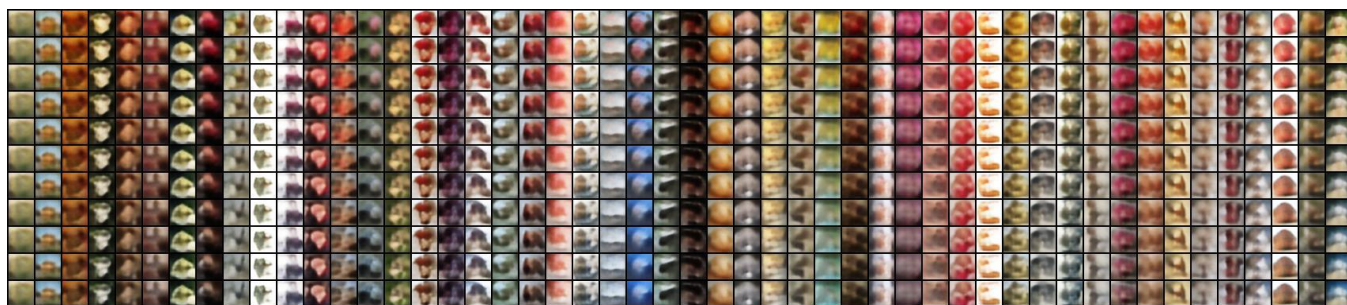


(c) Creation

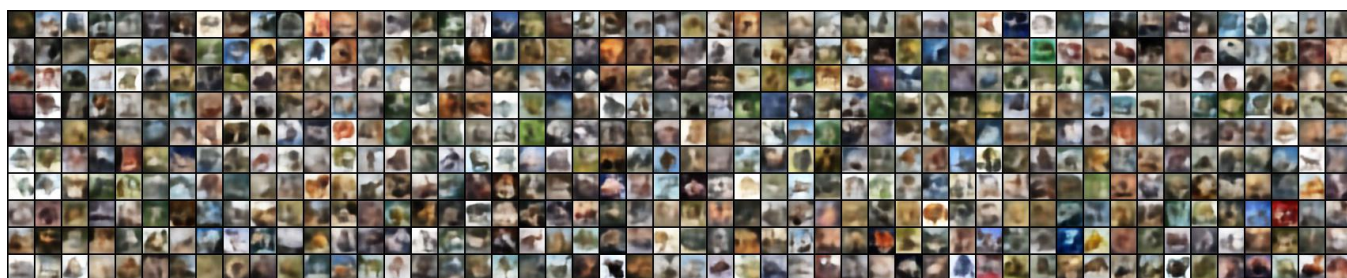
Fig. 22: (a) Generation (b) Transition (c) Creation from MCVAE trained with CIFAR100 dataset.



(a) Generation



(b) Transition



(c) Creation

Fig. 23: (a) Generation (b) Transition (c) Creation from CVAE trained with CIFAR100 dataset.

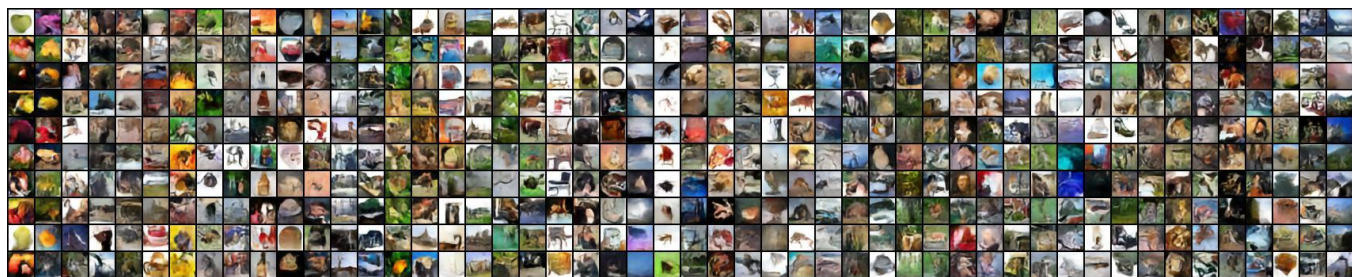


(a) Generation

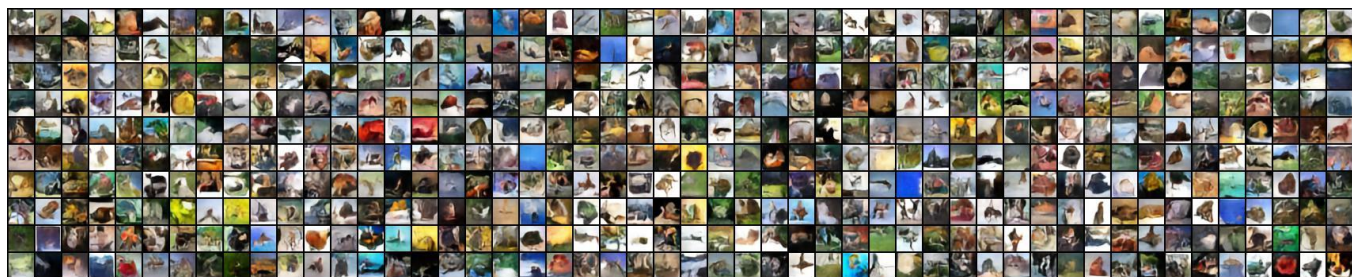


(b) Creation

Fig. 24: (a) Generation (b) Transition (c) Creation from MCPixelCNN trained with CIFAR100 dataset.



(a) Generation

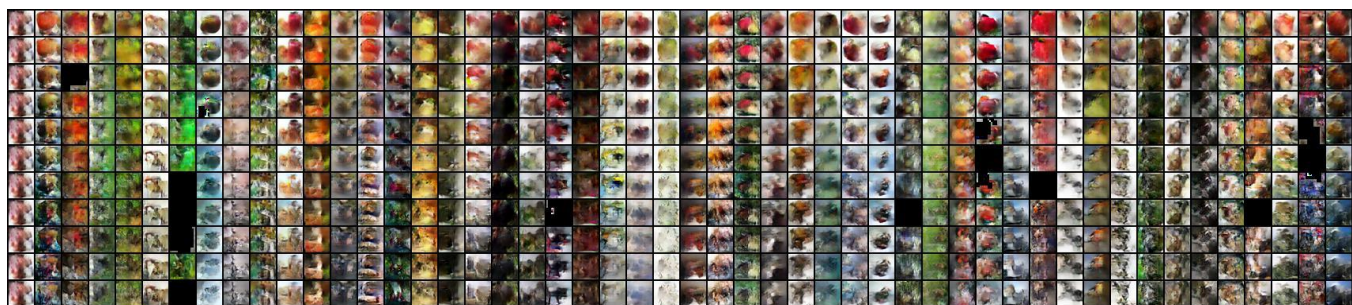


(b) Creation

Fig. 25: (a) Generation (b) Transition (c) Creation from CPixelCNN trained with CIFAR100 dataset.



(a) Generation

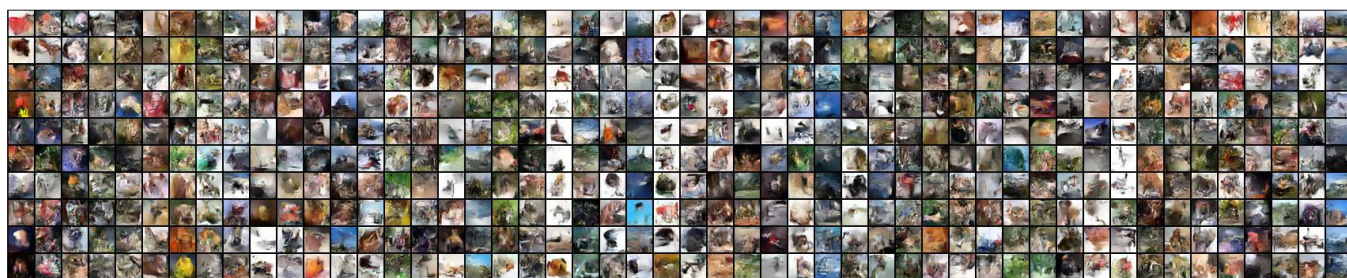


(b) Transition

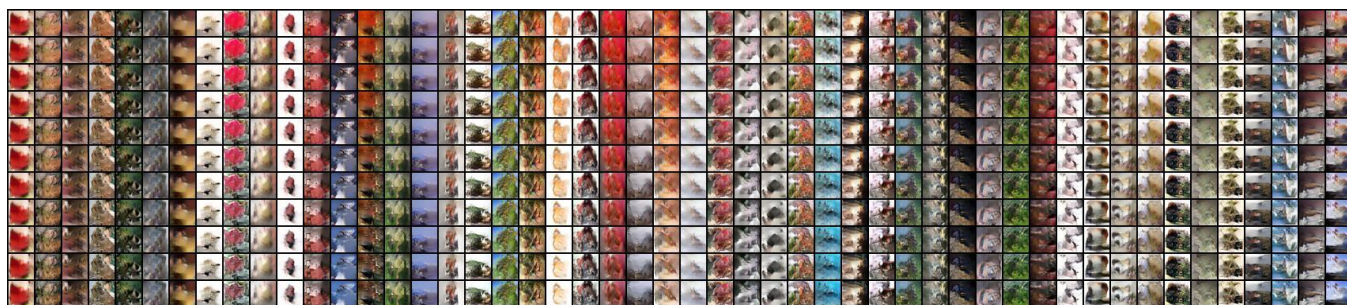


(c) Creation

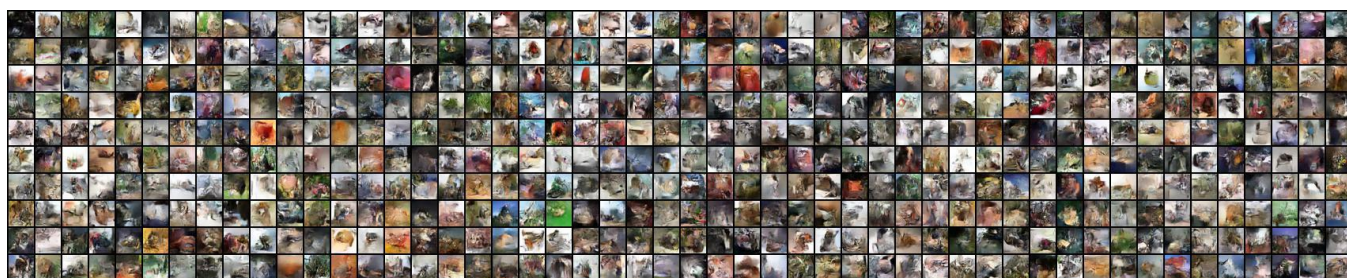
Fig. 26: (a) Generation (b) Transition (c) Creation from MCGlow trained with CIFAR100 dataset.



(a) Generation

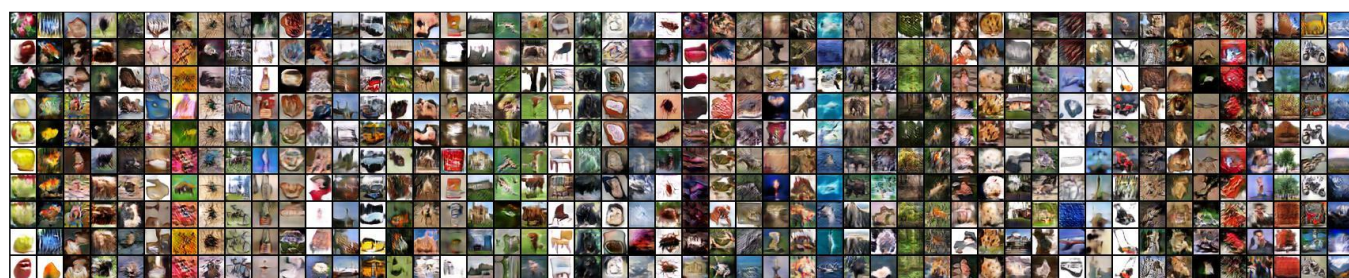


(b) Transition



(c) Creation

Fig. 27: (a) Generation (b) Transition (c) Creation from CGlow trained with CIFAR100 dataset.



(a) Generation



(b) Transition



(c) Creation

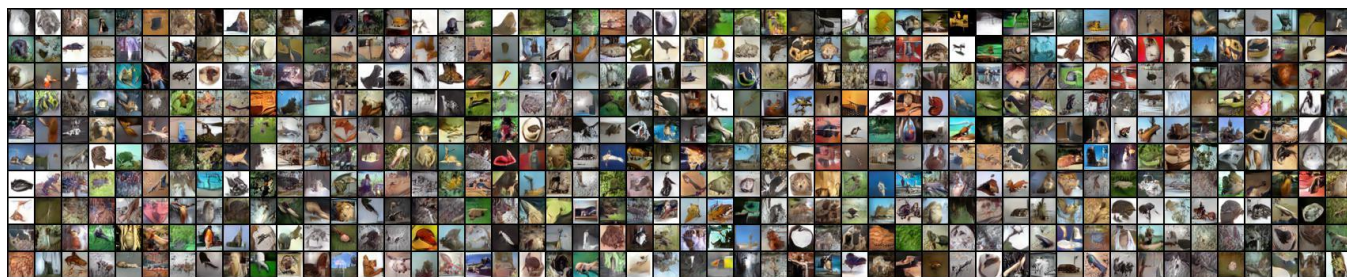
Fig. 28: (a) Generation (b) Transition (c) Creation from MCGAN trained with CIFAR100 dataset.



(a) Generation

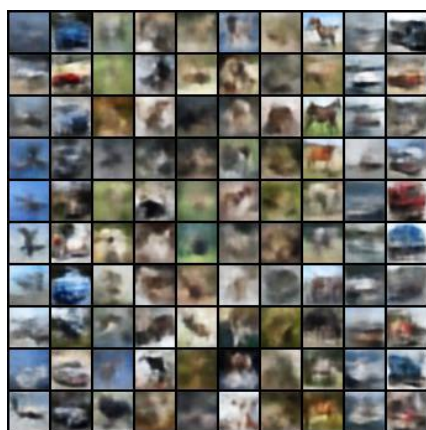


(b) Transition



(c) Creation

Fig. 29: (a) Generation (b) Transition (c) Creation from CGAN trained with CIFAR100 dataset.



(a) Generation



(b) Transition



(c) Creation

Fig. 30: (a) Generation (b) Transition (c) Creation from MCVAE trained with CIFAR10 dataset.

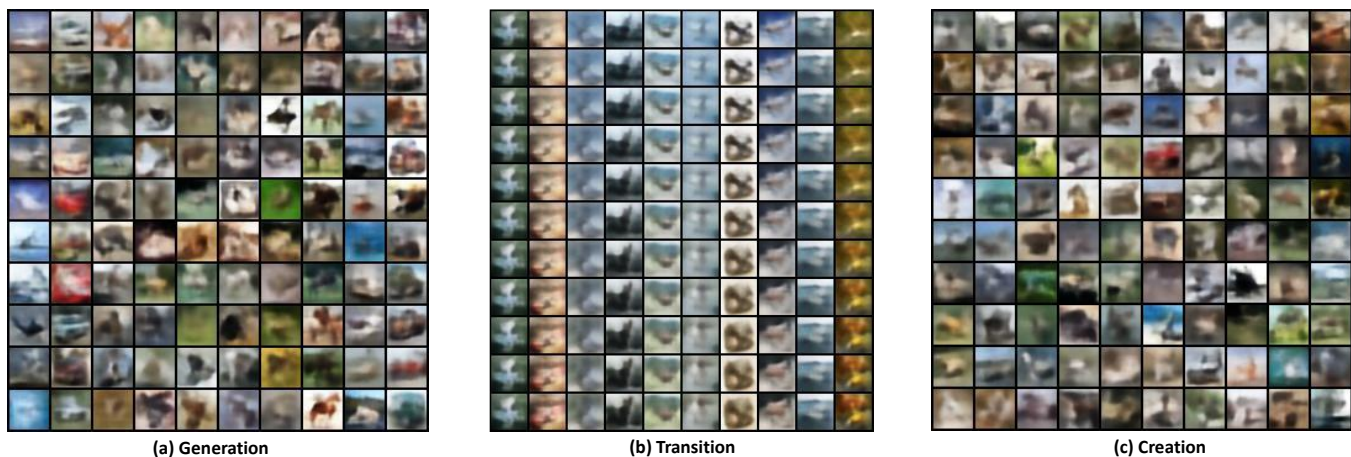


Fig. 31: (a) Generation (b) Transition (c) Creation from CVAE trained with CIFAR10 dataset.

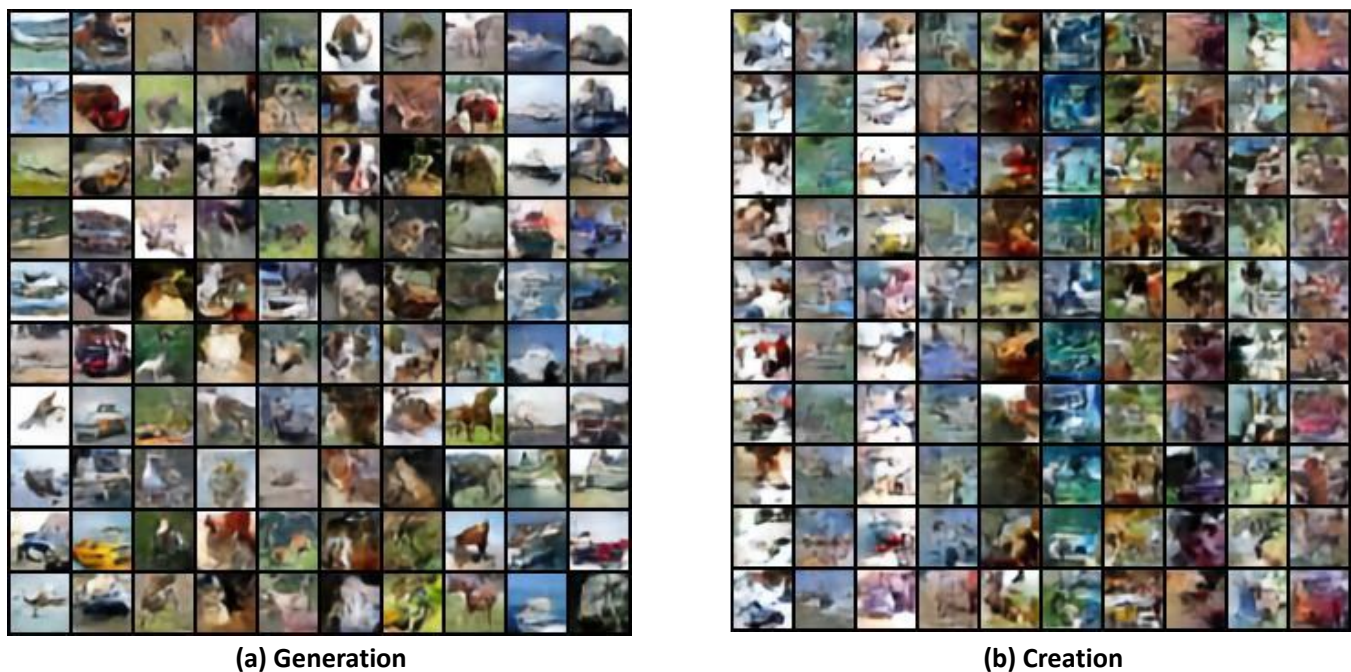
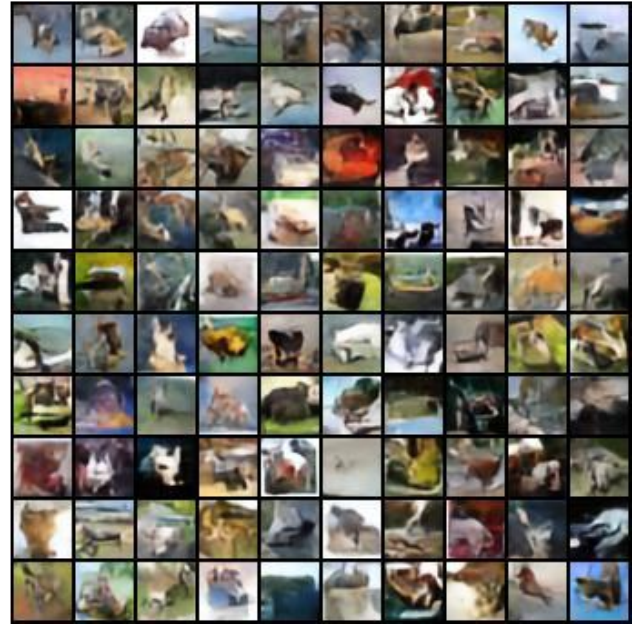


Fig. 32: (a) Generation (b) Transition (c) Creation from MCPixelCNN trained with CIFAR10 dataset.



(a) Generation

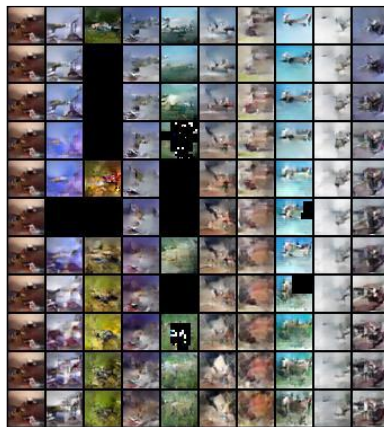


(b) Creation

Fig. 33: (a) Generation (b) Transition (c) Creation from CPixelCNN trained with CIFAR10 dataset.



(a) Generation



(b) Transition



(c) Creation

Fig. 34: (a) Generation (b) Transition (c) Creation from MCGlow trained with CIFAR10 dataset.

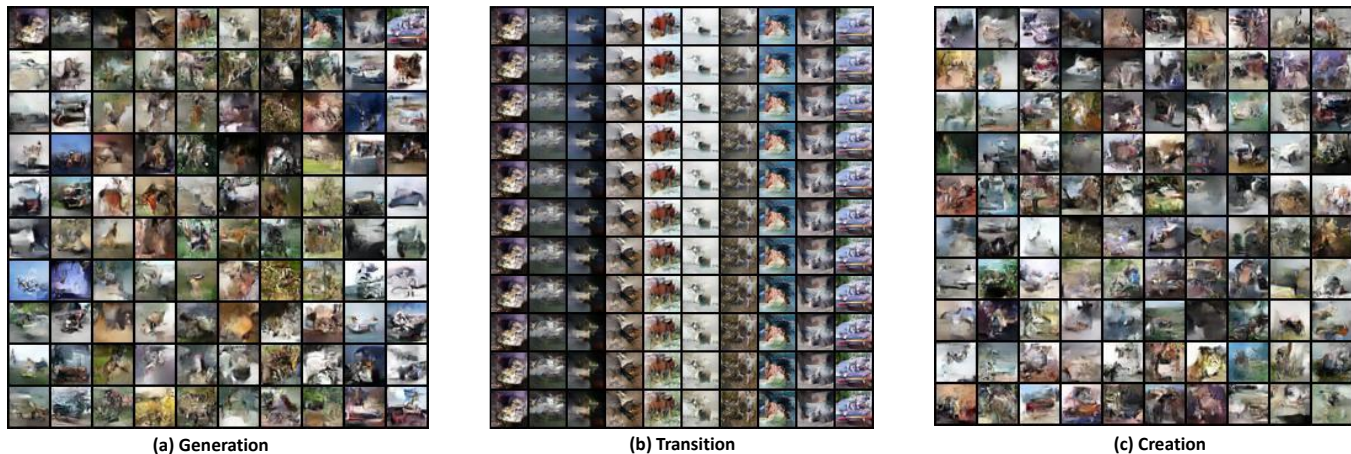


Fig. 35: (a) Generation (b) Transition (c) Creation from CGlow trained with CIFAR10 dataset.

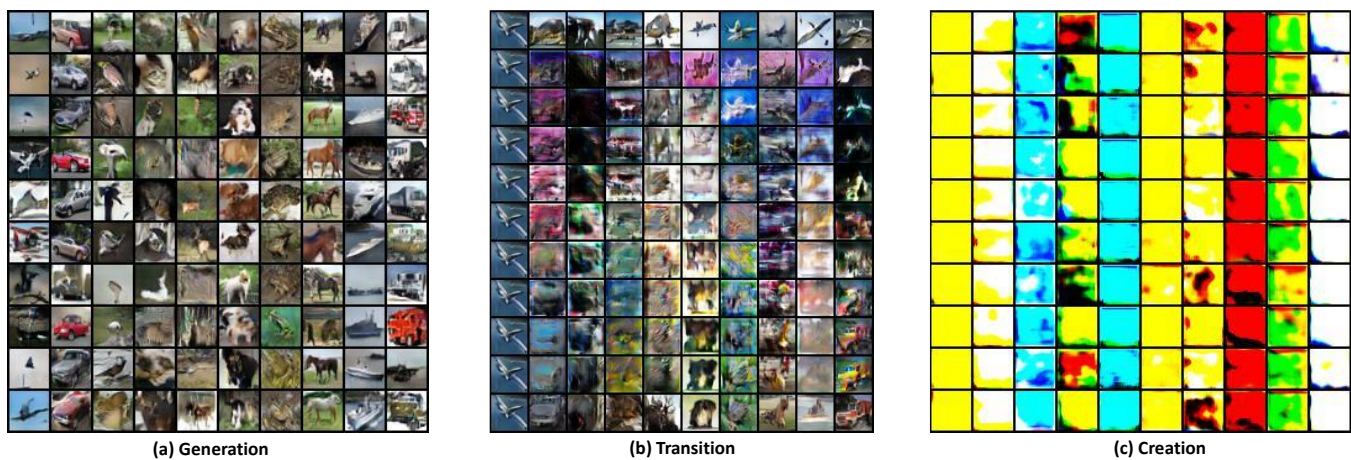


Fig. 36: (a) Generation (b) Transition (c) Creation from MCGAN trained with CIFAR10 dataset.

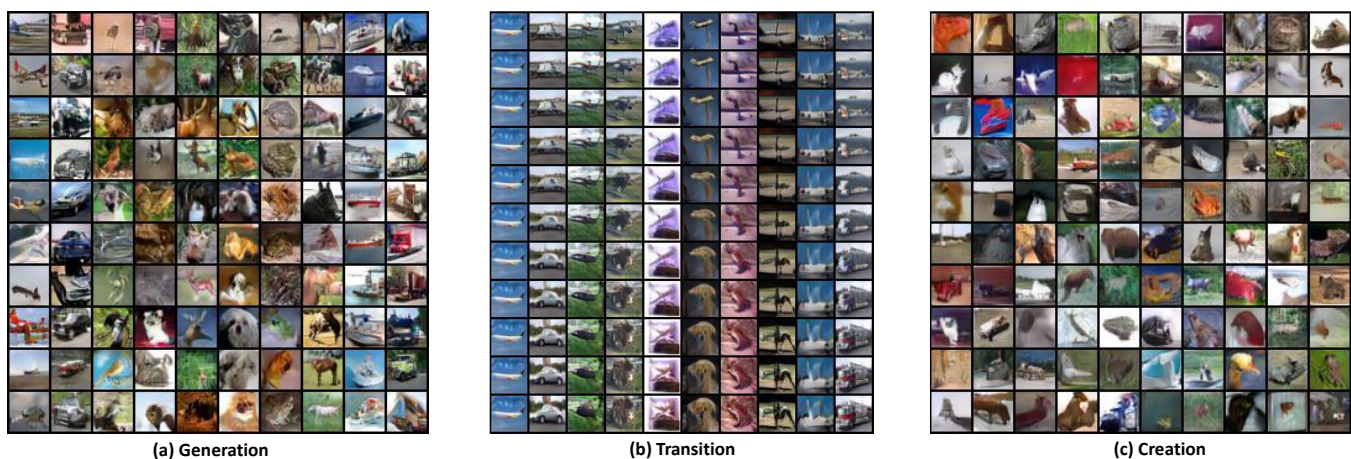


Fig. 37: (a) Generation (b) Transition (c) Creation from CGAN trained with CIFAR10 dataset.